Liquid Crystals
Publication details, including instructions for authors and subscription information:
http://www.informaworld.com/smpp/title~content=t713926090

Investigations of polarization profiles in sandwich cells containing a liquid crystalline polymer by using the heat wave method (LIMM)

M. Steffen[a]; P. Bloss[a]; H. Schäfer[a]; M. Winkler[a]; D. Geschke[a]
[a] Universität Leipzig, Fakultät für Physik und Geowissenschaften, Institut für Experimentelle Physik I, Leipzig, Germany

To cite this Article Steffen, M. , Bloss, P. , Schäfer, H. , Winkler, M. and Geschke, D.(1995) 'Investigations of polarization profiles in sandwich cells containing a liquid crystalline polymer by using the heat wave method (LIMM)', Liquid Crystals, 19: 1, 93 — 97
To link to this Article: DOI: 10.1080/02678299508036724
URL: http://dx.doi.org/10.1080/02678299508036724

LIQUID CRYSTALS, 1995, VOL. 19, NO. 1, 93–97

Investigations of polarization profiles in sandwich cells containing a liquid crystalline polymer by using the heat wave method (LIMM)

by M. STEFFEN, P. BLOSS*, H. SCHÄFER, M. WINKLER, and D. GESCHKE

Universität Leipzig, Fakultät für Physik und Geowissenschaften,
Institut für Experimentelle Physik I, Abteilung Polymerphysik,
Linnéstraße 5, D-04103 Leipzig, Germany

(*Received 29 October 1994; accepted 22 December 1994*)

The laser intensity modulation method (LIMM) was applied to the investigation of polarization distributions in sandwich cells of a side chain liquid crystalline polymer (LCP). The thermal poling procedure using a pulsating electric field was carried out for the nematic phase at 80°C. After cooling down the samples to room temperature T_R (i.e. below the glass transition temperature, T_g) a rather perfect alignment of the side chains could be obtained. Our first LIMM investigations at T_R show a nearly homogeneous polarization profile in the LCP layer.

1. Introduction

Much attention has been focused in recent years on thermotropic liquid crystalline side chain polymers which have come to prominence due to their intrinsic interest as a new class of materials with great potential for use in various application areas [1]. In LCPs, the properties of low molecular weight liquid crystals are combined with those of polymers, such as flexibility and easy processing. In the special case of displays, which have to be considered as multilayer systems, polymer interfaces are used to induce a pre-alignment of the first molecular layer [2]. In order to study the electric behaviour Sugimura *et al.* [3], proposed, for example, a 4-component circuit with a polymer interface.

The aim of the present paper is to investigate polarization profiles in homeotropically oriented sandwich cells of a commercial LCP (trade name LCP 105), using the LIMM technique which we have successfully employed in the case of polyvinylidene fluoride (PVDF) and Teflon^R FEP [4–6].

2. Experimental

2.1. *Samples*

The liquid crystalline polymer (LCP) was contained in a sandwich cell (see figure 1). The front and rear plates, as well as the spacer ring, consist of polyimide (PI) foils (Kapton^R) available from Krempel (Vaihingen, Germany). The cover foils (7·5 μm thick) and the spacer material (25 μm) consist of Kapton^R 30 HN and Kapton^R 50 HN, respectively. The thermal parameters of the PI foils are [7]: heat conductivity $\kappa_{PI} = 0{\cdot}12\,J\,s^{-1}\,m^{-1}\,K^{-1}$ and diffusivity $\chi_{PI} = 77 \times 10^{-9}\,m^2\,s^{-1}$ (similar parameters for both materials).

The LCP material was purchased from Merck Ltd, England. The first description was given by LeBarny *et al.* [8]. It was characterized by the code LCP 105, batch number 069123; the glass transition temperature $T_g = 35{\cdot}3$°C, the nematic–isotropic phase transition point $T_{NI} = 125{\cdot}5$°C, and the averages of the molar mass $\bar{M}_n = 6050\,g\,mol^{-1}$ (number average; this leads to an average number of monomer units $n = 16{\cdot}7$ in the molecule) and $\bar{M}_w = 9040\,g\,mol^{-1}$ (weight average). The chemical structure is given in figure 2. No monomer could

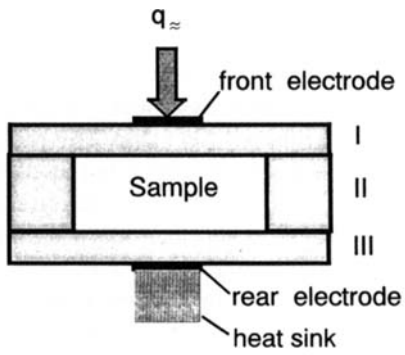

Figure 1. Scheme of the sandwich cell. I: PI front plate (thickness 7·5 μm), II: PI spacer (25 μm), III: PI rear plate (7·5 μm), $q_\approx$: incident heat flux. The central electrodes and the LCP material contained in the sandwich cell have diameters of 2 mm and 10 mm, respectively.

* Author for correspondence.

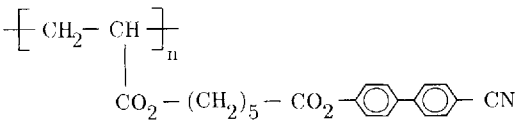

Figure 2. The structure of the liquid crystalline polymer with the trade name LCP 105. $\bar{M}_n = 6050\,g\,mol^{-1}$, $\bar{M}_w = 9040\,g\,mol^{-1}$, $n = 16{\cdot}7$ units (average).

be detected by gel permeation chromatography. These data were available from the accompanying data sheet.

Before making the sandwich cell, the cover foils were vacuum deposited with a gold layer (about 100 nm thickness) through a mask on one side. These metal coatings are shown outside the sandwich structure. In this manner, the samples were setup for LIMM measurements.

2.2. *Poling procedure*

The poling procedures were carried out as follows: first the samples were heated up in an oven to the poling temperature $T_P = 80°C$. A pulsating electric field with a positive voltage $U_P = +500\,V$ was now applied (frequency 100 Hz, duration 10 min) to side L in our nomenclature. This poling procedure was performed with the samples in the nematic phase, $T_P < T_{NI}$. Then the samples were cooled down to room temperature $T_R = 25°C$ (below T_g) in the presence of the applied electric field. The heating and cooling processes were carried out at $\approx 1\,K\,min^{-1}$.

We verified the alignment of the side chains towards the electric field by NMR experiments [9]. By means of polarization microscopy, a clear LCP layer was observed over several weeks. Therefore, we have assumed that the orientation of the LCP was stable over this time range. The LIMM measurements were carried out at room temperature T_R.

2.3. *LIMM measurements*

The principles of the laser intensity modulation method (LIMM) are only briefly presented here (for details see elsewhere [4, 10]). A sample possessing opaque metal layers on its surface (thickness about 100 nm) is irradiated by an intensity modulated laser beam. This metal layer acts simultaneously as a light absorber and an electrode. The intensity changes sinusoidally (modulation frequency f), and therefore, in the front electrode a thermal wave is generated, which penetrates into the sample. For low modulation frequencies, the penetration length of the thermal waves δ is great (for $f = 1$ Hz, for polymer material typically 150 μm). With increasing f, the heated range in the sample is more and more concentrated near the front surface.

The transient temperatures of the sample surfaces can be measured in a bolometer arrangement [11]. For free standing samples (low heat transfers on both sides), the effect of the 'thermal scan' of the sample by means of thermal waves can be easily explained. At low modulation frequencies, where the thermal waves reach the rear side of the sample, the sample is homogeneously heated over the whole thickness. This means that both surface temperatures are nearly identical. With increasing modulation frequency, the thermal waves cannot reach the rear side, and therefore, the temperature on the rear side decreases drastically with respect to the temperature on the front side. For further details see, for example, [11].

The pyroelectricum can be considered as a multilayer system: each layer possesses a pyroelectric coefficient $g(z)$ and experiences a temperature increase of $T(f, z)$, where z is the coordinate perpendicular to the sample surface. The measured signal is the short-circuit current between the front and the rear electrode $I_P(f)$, and is therefore determined by a summation (or integration) over all layers. The contribution of each layer is given by the term $g(z)[j2\pi f T(f, z)]$, where the second term is the change of $T(f, z)$ with time: $\partial/\partial t = j2\pi f$; j is the imaginary unit.

Only the heated part of the sample contributes to $I_P(f)$. Hence, the sample can be scanned by variation of the modulation frequency. Note that the space charges also contribute to the pyroelectric signal due to changes of the sample thickness L and permittivity $\varepsilon_0\varepsilon$.

In our measurements, the samples were thermally contacted on the rear side in order to prevent unwanted mechanical vibrations of the sample in the high frequency range ($f > 1$ kHz) [12]. Such vibrations cause strong electrical signals which make the pyroelectric spectrum unsuitable for further treatment. The limits for the modulation frequencies are: $f_{min} = 3{\cdot}1$ Hz and $f_{max} = 31$ kHz. For f_{min}, the thermal waves reach the rear side of the sample. The current was measured for 200 frequencies per frequency decade (chosen in a statistical manner according to an idea of Lang [13]), and then it was corrected in phase and amplitude. The noise (related to the maximum absolute value of the current) was found to be ≈ 5 per cent. The amplitudes of the pyroelectric signal were $< 0{\cdot}5$ pA. These low signals make the experiments time-consuming (up to 2 d for one spectrum). Our equipment is described in detail elsewhere [4].

2.4. *The deconvolution of the LIMM spectra*

The measured pyroelectric current, $I_P(f)$, and the spatial distribution function $r(y)$ are linked by a Fredholm integral equation of the first kind [10, 14]

$$I_p(f) = A \int_0^1 r(y) F(f, y)\, dy,$$
$$r(y) = g(y) - (\alpha_z - \alpha_v)\varepsilon\varepsilon_0 E(y). \tag{1}$$

Here y, A, α_z, and α_v are the relative coordinate ($y = z/L$), the irradiated area, the relative temperature coefficients of

the thickness and the permittivity $\varepsilon_0\varepsilon$, respectively. $r(y)$ contains the contributions of the true pyroelectricity $g(y)$ and the electric field $E(y)$ (due to space charges and due to residual polarization [4, 14]).

The integral kernel in equation (1) is represented by the thermal force $F(f,y) = j2\pi fT(f,y)$. It is already known that LCPs with such polar side chain groups are adsorbed on PI foils [15, 16, 17]. Hence, we have neglected the heat transfer between the LCP and the PI cover foils. Furthermore, we assume similar thermal parameters (κ and χ) for the LCP and PI foils, and in consequence, we have applied the solution of the heat conduction equation for one unified layer, $T(f,y)$ (the periodic part of the solution, irradiation from $y = 1$) [4]

$$T(f,y) = \frac{q_\sim \eta_a}{\kappa K} \frac{ch(KLy) + \dfrac{H_0}{\kappa K} sh(KLy)}{\left(1 + \dfrac{H_0 H_L}{\kappa^2 K^2}\right) sh(KL) + \dfrac{H_0 + H_L}{\kappa K} ch(KL)}, \tag{2}$$

where $q_\sim$, η_a, K, H_0, and H_L are the amplitude of the incident heat flux, the absorptivity, the heat conductivity, the wavevector of the thermal waves $= (1 + j)/\delta$, the heat transfer coefficients on the rear ($y = 0$) and the front side ($y = 1$), respectively. δ is the penetration length of the thermal waves, $\delta = \sqrt{[\chi/(\pi f)]}$.

The solution $r(y)$ is determined by means of the Tikhonov regularization method (with respect to LIMM, see for example, [4, 10, 12, 18]). We have used the second derivative of the spatial function $r(y)$ in the regularization term, favouring smooth spatial distributions. The spatial grid distribution was linear with $N = 51$ grid points. In the deconvolution process, the error in the thermal parameters (χ, H_0) was eliminated by means of an iteration procedure described elsewhere [12, 18].

3. Results and discussion

For the determination of the detection level of these samples, an unpoled sample was exposed to the same thermal treatment as the poled sample. We found an amplitude of the pyroelectric current smaller than 20 fA independent of the modulation frequency (for $f = 3\,\text{Hz} \ldots 30\,\text{kHz}$). Therefore, this value can be considered as a detection limit for our equipment.

In figure 3 the pyroelectric spectrum, together with the residues (the curves near zero) are shown, if side $y = 0$ was irradiated, that is, the side connected to ground potential during the poling process. One can see a very low signal strength in the high frequency part of the spectrum, where the thermal waves cannot reach the LCP layer. Therefore, in the PI-cover layers, the spatial distribution is ≈ 0.

The spatial distribution functions $r(y)$, which are determined separately from the real and the imaginary part of the LIMM spectrum are shown in figure 4. The spatial functions are normalized with respect to their peak values. The adaptation of the spectra was exhaustive, and this leads to noise-like residues (see figure 3). The residue is the difference between the measured and the recalculated current.

The parameters used in the deconvolution are: (1) $L = 40\,\mu\text{m}$, (2) $\chi = 80 \times 10^{-9}\,\text{m}^2\,\text{s}^{-1}$, (3) $\kappa = 0{\cdot}12\,\text{J}\,\text{s}^{-1}\,\text{m}^{-1}\,\text{K}^{-1}$, (4) $H_0 = 10^4\,\text{J}\,\text{s}^{-1}\,\text{m}^{-1}\,\text{K}^{-2}$, and (5) $H_L = 5\,\text{J}\,\text{s}^{-1}\,\text{m}^{-2}\,\text{K}^{-1}$ (free standing air). L was found by means of a mechanical thickness measurement; χ and H_0 are determined in the deconvolution process (see above). χ coincides with the value for PI (see above), which can be considered as an indication that the one layer treatment is sufficient in the deconvolution process (that is, one homogeneous layer with homogeneous thermal

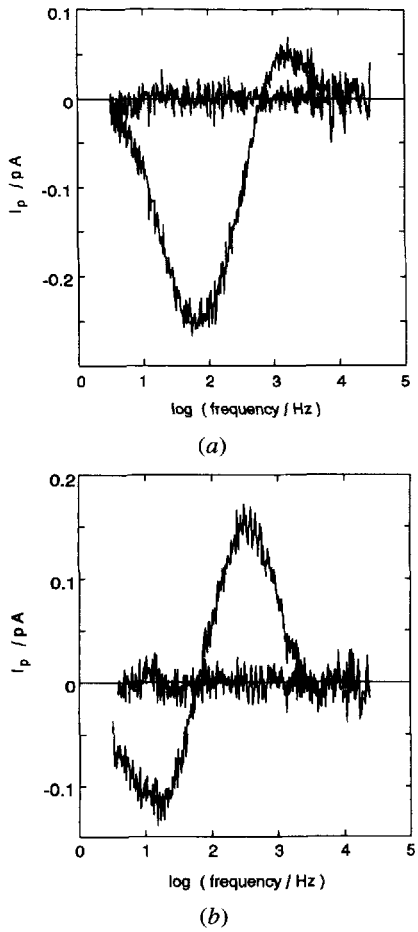

Figure 3. Pyroelectric spectrum obtained from the poled sandwich cell if the irradiation was done from $y = 0$, the side where the ground potential was applied to the sample during the poling process. The curves near zero represent the residues showing exhaustive adaptation. On the left and right sides, the real and the imaginary parts are shown, respectively.

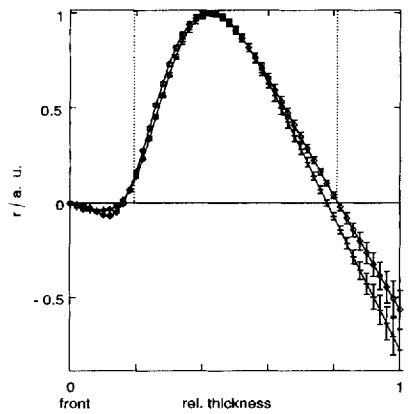

Figure 4. The spatial distribution function $r(y)$ obtained from the spectral which are shown in figure 3. The rectangular profile is given in a dotted line, if for both PI cover sheets and the LCP layer, 7·5 μm and 25 μm were used, respectively.

properties). Anyway, improvement of the residues is not expected: for differentiation of the thermal properties of the cover and the LCP layer, the noise is not small enough. The value of H_0 is typical of our measurements [5, 6].

In figure 4 one can see a nearly homogeneous spatial distribution $r(y)$ in the LCP layer, in the sense of spatial resolution of LIMM. The spatial function $r(y)$ should first be discussed, when we give some comments on the origins of $r(y)$.

An idealized rectangular spatial distribution is marked by the dotted line. However, such a rectangular spatial distribution cannot be obtained because of the restriction of smooth distributions, which is the only assumption used. In principle a fit of the spectrum with a rectangular spatial distribution (with 3 parameters: 2 borders and the amplitude of the polarization zone) is possible, but such strong and from the outset limited assumptions seem to be doubtful.

For our noise amplitudes (≈ 5 per cent), the deconvolution delivers significant results up to approximately the first half of the thickness, with respect to the front side. The decreasing spatial resolution with increasing distance from the irradiated side is visualized by error bars in figure 4. The negative value of $r(y)$ near the rear side seems not to be realistic and can be attributed to the low spatial resolution near the rear side.

If the residual polarization is locally compensated by the charge density [i.e. $E(y) = 0$], the function $r(y)$ reduces to the pyroelectric coefficient $g(y)$ [see equation (1)] [14]. In this case, for the quantification of the mean value of the pyroelectric coefficient, a comparison with data which we have obtained from commercial Solvay^R PVDF is advantageous. For Solvay^R PVDF possessing $g = 25\,\mu C\,m^{-2}K^{-1}$ (available from the accompanying data material), we have found a signal strength of ≈ 150 pA for the same experimental conditions. Hence, for this LCP material, the mean pyroelectric coefficient is approximately 150 times smaller than for Solvay^R PVDF, $g \approx 170\,nC\,m^{-2}K^{-1}$. The signal decrease due to the PI cover layers was taken into account.

Space charges (for example, due to impurities) could be frozen-in near both the PI cover sheets during cooling to room temperature in the presence of an applied electric field. They could also cause a constant electric field $E(y)$, and therefore a constant $r(y)$. Note that a constant space charge density over the LCP layer causes an electric field with a constant slope in this layer. However, if the electric conductivity κ_{el} of the LCP material is high enough, such charge separation on both LCP surfaces should not be possible. We have determined $\kappa_{el} \approx 3 \times 10^{-12}\,\Omega^{-1}\,m^{-1}$. A rough estimation of a time τ, in which a possible charge layer on the surfaces of the LCP decays, can be carried out by means of $\tau = \varepsilon_0\varepsilon/\kappa_{el}$ (see, for example, in [19]). With $\varepsilon \approx 6{\cdot}5$ determined by us, the time τ is < 20 s, and therefore, we assume that the contribution of such charge layers to the spatial function $r(y)$ can be neglected.

The orientation order of LCP 105 after poling has been studied extensively by NMR investigations [9]. The threshold field strength for an electrically induced Fréederickz transition is given by

$$E_0 = \frac{\pi}{d}\sqrt{\left(\frac{K_{11}}{\varepsilon_0|\Delta\varepsilon|}\right)} \tag{3}$$

where d is the thickness of the LCP layer, K_{11} the splay elastic constant, $\Delta\varepsilon$ the anisotropy of the dielectric constant and ε_0 the absolute permittivity. Under poling conditions, in every case, the relation $E > E_0$ holds.

The NMR resonance line is, for the simplest case of a two-proton system, a doublet according to the two orientations of a proton dipole in the external B_0 field. Under conditions of transverse anisotropy, i.e. (i) rapid rotation of the side chain units around the axis, (ii) within a domain the chain axes are uniformly distributed on a cone around the director axis, and (iii) the director distribution is axially symmetric around a preferred axis in the sample (average director axis) one gets

$$\Delta\nu = \frac{3\mu_0}{16\pi^2}\frac{\gamma^2\hbar}{\langle r\rangle^3}\frac{1}{2}(3\cos^2\phi - 1)S \tag{4}$$

Here $\Delta\nu$, r, γ, $\hbar$, S, and ϕ are the line splitting, the internuclear proton vector, the gyromagnetic ratio of protons, Planck's constant divided by 2π, the parameter of the orientational order, and the angle between B_0 and the preferred axis, respectively. For further details see [9].

It could be shown that a rather perfect alignment with $S \approx 0{\cdot}85$ has been reached. Figure 5 shows the temperature dependence of $\Delta\nu$ and S. Sufficient polarization magnitudes could only be obtained in cases with $S \approx 1$,

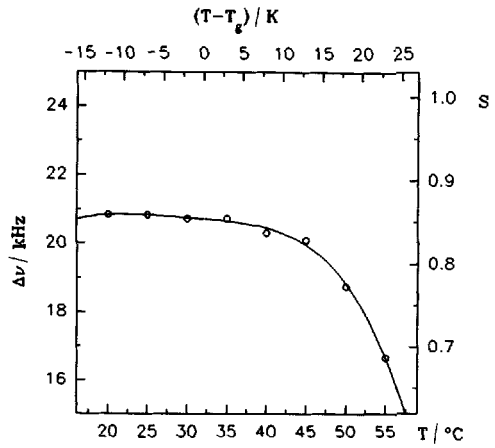

Figure 5. The temperature dependence of $\Delta\nu$ and S.

demonstrating a strong connection between electrical and orientational effects. Further investigations are in progress.

4. Conclusions

In the present paper we have presented our first results for a polarization profile in a LCP layer incorporated in a sandwich cell. We have found a net polarization existing in the LCP layer, which is homogeneously distributed over this layer. Because the electrical conductivity of our LCP material is sufficiently large, a possible contribution of the electric field to the determined spatial function can be neglected.

NMR measurements delivering the mean value of the orientation parameter over the thickness have shown a rather perfect alignment of the polar side chains. However, the NMR can only detect the direction, but not the sense of the direction (in contrast to the pyroelectric measurements) of the polarization vector. Obviously, the pyroelectric measurements give additional information about the orientation of dipoles.

The Kapton^R films used in the present study were kindly made available free of charge by DuPont de Nemours Germany. Financial support by the Deutsche Forschungsgemeinschaft within the research projects No. B1376/1-2 and No. Ge718/1-2 is gratefully acknowledged.

References

[1] McArdle, C. B., 1989, *Side Chain Liquid Crystal Polymers* (Blackie & Son Ltd.), Chap. 11.
[2] Johannesmann, D., Zhou, H., Sendekazer, P., Wierenga, H., Myrold, B. O., and Shen, Y. R., 1993, *Phys. Rev.* E, **48,** 1889.
[3] Sugimura, A., Takahashi, Y., and Zhong-can, O. Y., 1993, *Jap. J. appl. Phys.*, **32,** 116.
[4] Bloß, P., and Schäfer, H., 1994, *Rev. Sci. Instr.*, **65,** 1541.
[5] Bloß, P., Steffen, M., and Schäfer, H., 1994, *Proceedings of the 8th International Symposium on Electrets*, edited by J. Lewiner, D. Morisseau, and C. Alquié, Paris, p. 194.
[6] Bloß, P., Steffen, M., and Schäfer, H., 1994, (in preparation).
[7] Available from the DuPont data material.
[8] LeBarny, P., Dubois, J.-C., and Noël, C., 1986, *Polymer Bull.*, **15,** 341.
[9] Winkler, M., Geschke, D., and Holstein, P., 1994, *Liq. Crystals*, **17,** 283.
[10] Lang, S. B., 1991, *Ferroelectrics*, **118,** 343.
[11] Bauer, S., and Bloß, B., 1990, *Ferroelectrics*, **106,** 393.
[12] Steffen, M., Bloß, P., and Schäfer, H., *Rev. Sci. Instr.* (submitted).
[13] Alquie, C., Lang, S. B., and Lewiner, J., 1991, *Proceedings of the 7th International Symposium on Electrets*, edited by R. Gerhard-Multhaupt, W. Künstler, L. Brehmer, and R. Danz, Berlin, p. 331.
[14] Ploß, B., Emmerich, R., and Bauer, S., 1992, *J. appl. Phys.*, **72,** 5363.
[15] Berreman, D. W., 1972, *Phys. Rev. Lett.*, **28,** 1683.
[16] Seary, J. M., Goodby, J. W., Kmetz, A. R., and Patel, J. S., 1987, *J. appl. Phys.*, **62,** 4100.
[17] Murata, M., Yoshida, E., Uekita, M., and Tawada, Y., 1993, *Jap. J. appl. Phys.*, **32,** L676.
[18] Steffaen, M., Bloß, P., and Schäfer, H., 1994, *Proceedings of the 8th International Symposium on Electrets*, edited by J. Lewiner, D. Morisseau, and C. Alquié, Paris, p. 200.
[19] Sessler, G. M., 1980, *Electrets* (Springer-Verlag), Chap. 2.6.4.